

# **Is Biofeedback Training of Ownership Perceptions Possible? EEG Classification of Volitional Hand-Ownership using Common Spatial Patterns**

---

Terence Mayne

A Thesis Submitted for the Degree of Master of Science  
at the University of Otago, Dunedin, New Zealand

30 May, 2016

2.1.8	Trial Structure .....	21
2.1.9	Internal Guidance Phase .....	22
2.1.10	External Guidance Phase .....	22
2.1.11	Post-trial Phase.....	23
2.1.12	Trial Blocks.....	23
2.2	Ownership–Detachment Classification.....	24
2.2.1	Discriminatory Feature Adaption Using Common Spatial Patterns	24
2.2.2	Machine Learning Using Linear Discriminant Analysis.....	25
2.2.3	Classifier Implementation .....	26
2.2.4	Classification Pipeline .....	26
2.2.5	Classification Regimes .....	27
2.2.6	Software and Scripting of Classification Pipeline.....	29
2.2.7	EEG Pre-processing .....	30
2.2.8	Artifact Subspace Reconstruction.....	30
2.2.9	Classifier Creation Parameters .....	30
2.2.10	Independent Component Analysis .....	31
2.2.11	Online Simulation .....	31
2.2.12	Performance Evaluation and Statistical Analyses.....	31
3	RESULTS .....	36
3.1	Classification Performance.....	36
3.2	One-sample T-tests .....	36
3.2.1	Internal Guidance .....	37
3.2.2	External Guidance .....	37
3.3	Distribution Plots .....	39
3.3.1	Participant-independent and Participant-dependent Distributions .	39
3.3.2	Internal and External Distributions.....	40
3.4	Correlations .....	41
3.4.1	Participant-independent–Participant-dependent Performance .....	42
3.4.2	Internal–External Guidance Performance.....	43
3.5	ANOVA.....	44
3.6	Biophysical Features .....	45
3.6.1	CSP Patterns and Filters .....	45

## Glossary

**Accuracy** – The rate at which a classifier can successfully label unlabelled-EEG.

**Augmented reality** – Virtual reality where ‘real’ visuals are intertwined with virtual objects.

**Biosignals** – Electrophysiological indicators of biological states and processes.

**Biofeedback (visual)** – The presentation of physiological signals to users to aid attempts to control their physiology. Visual feedback is relayed in the form of visual transitions that are reflective of a users’ physiology to improve user’s control of the physiological signal.

**Bottom-up** – Neural processes that build primary sensory input into abstract representations.

**Calibration** – The process of capturing labelled EEG data to train classifiers in an offline manner for subsequent use in online feedback.

**Classification** – The application of a classifier to unlabelled EEG to predict which physiological state or condition the participant was in.

**Classification regime** – Classification using a specific set of parameters to create the classifiers.

**Classifier** – A predictive algorithm, including feature extraction and machine learning constants that have been adapted by training on calibration EEG data.

**Classifier-training** – Adapting constants in the prediction algorithm using calibration EEG.

**Cognition** – The broad set of mind processes including attention and judgement.

**Cross-validation** – The partitioning of an offline EEG dataset into training and test sets to estimate the accuracy of a classifier during online EEG classification.

**Detachment** – The dissociation from any ownership perceptions of a body part.

**External** – Those cues derived from sensory inputs; presently through visual guides.

**Features** – Values extracted from the EEG intended to be most representative of the discrimination between the perceptual states under classification scrutiny.

shown to cause lasting improvements in the control of one's attention (Gevensleben et al., 2009).



**Figure 2. Biofeedback Training Illustration.** The user attends to the visual presentation of EEG biosignals to increase awareness of her mental state to aid control of it.

### 1.3.1 Improving Biofeedback using Spatial Filters and Machine Learning

An issue of EEG-based biofeedback is that the EEG signal lacks spatial resolution, largely because each electrode records a multitude of signals from disperse regions of cortex (Loo & Makeig, 2012; Makeig, Debener, Onton, & Delorme, 2004). Spatial filtering methods such as Common Spatial Patterns (CSP) (Blankertz, Tomioka, Lemm, Kawanabe, & Müller, 2008) and machine learning algorithms such as Linear Discriminant Analysis (LDA) (Vidaurre, Schlögl, Blankertz, Kawanabe, & Müller, 2008) can improve the accurate detection of specific EEG signals representing different physiological states. These methods are applicable in online conditions and have been suggested as a future direction in biofeedback application (Loo & Makeig, 2012). The present paradigm implements such methods in an offline calibration context; a background of these methods and how they are presently applied is given in “Ownership–Detachment Classification” of the Methods on page 24.

## 1.4 Possible Neural Targets of Ownership Biofeedback

A biofeedback training regime needs a reference biosignal to target (Jensen et al., 2013). That is, a biosignal must be found that has a functioning role in the mechanisms of the condition or symptoms of interest and is susceptible to user control. This signal needs to be identified and

## Introduction – Is Biofeedback Training of Ownership Perceptions Possible?

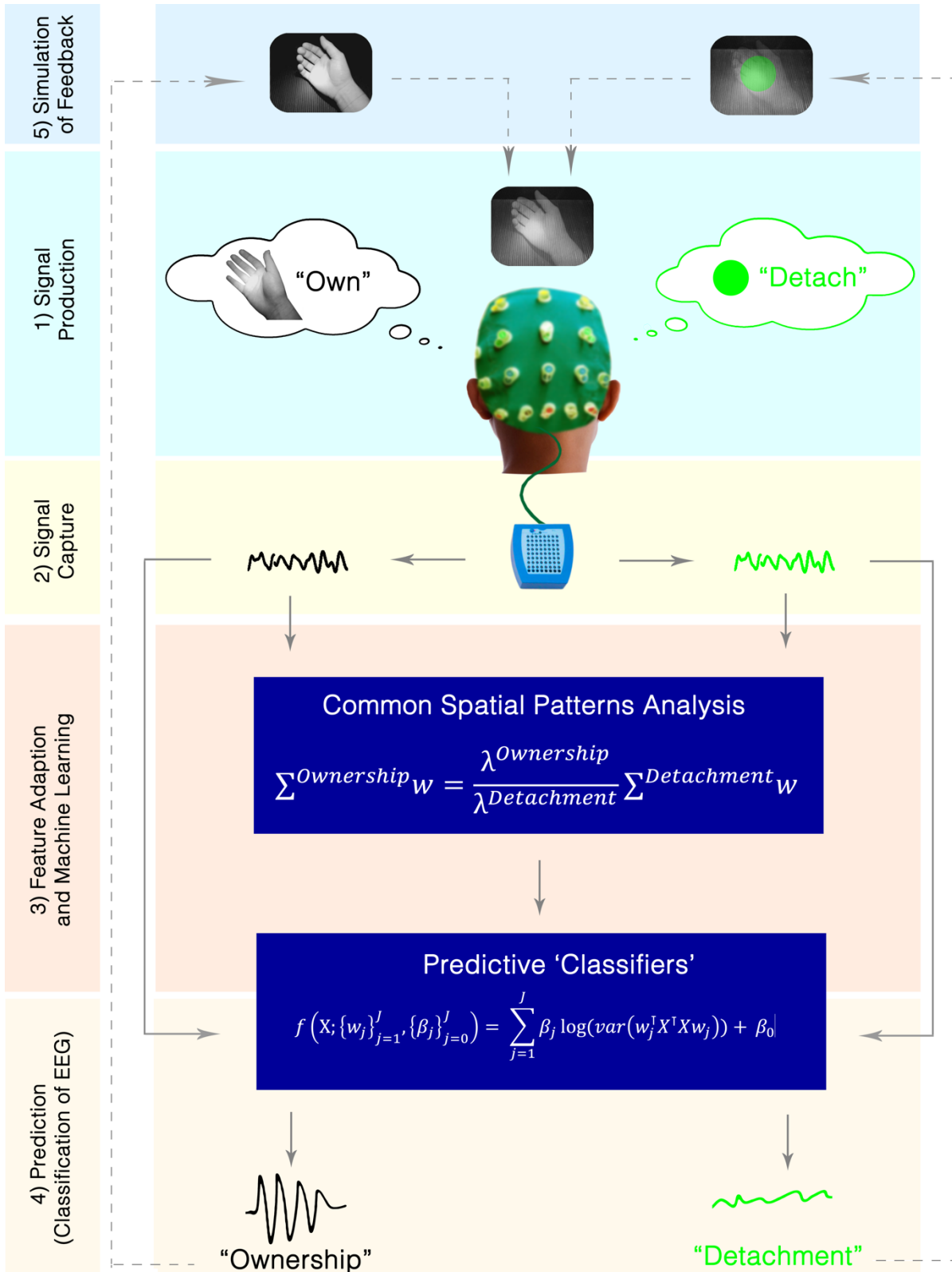


**Figure 3. Overview of Proposed Ownership-Detachment Biofeedback Pipeline.** The pipeline begins with signal production where the user attends to internal guides to produce ownership or detachment perceptions. The paradigm implemented in this thesis is offline calibration (steps 1-4), with a *simulation* of feedback (step 5). A follow-up online biofeedback task would involve steps 1, 2, 4 and 5 and use a predictive 'classifier' created in step 3 (during offline calibration). Description of the feature adaption and machine learning methods used to create predictive 'classifiers' to discriminate between ownership and detachment EEG can be found on page 24.

## 2 METHODS

### 2.1. Ownership–Detachment Calibration Task

The primary purpose of the task was to elicit and capture internally-generated perceptual states of ownership and detachment of a virtual hand to be used in a feasibility assessment of biofeedback training of these states. Therefore ownership and detachment states were captured in two phases – under volitional “internal” guidance and under feedback “external” guidance stimuli. The internal guidance condition consisted of a visual stimulus of a virtual hand that was *neutral* across ownership and detachment conditions. Contrarily, external guidance had visual stimuli that were *condition specific* with symbols of ownership composed of a fully opaque virtual hand stimulus and detachment symbols represented by a green distractor with the virtual hand having ‘disappeared’.

#### 2.1.1 Participants

Thirty-six undergraduate psychology students (29 female, 7 male, 2 left-handers) participated in the experiment. Age range was 18-26 with mean age of 20 years. One participant was removed from analyses due to missing data. Participants were remunerated with psychology course credits. Entire task duration was approximately 90 minutes for each participant.

#### 2.1.2 Virtual Box

A “virtual box” was constructed such that in a dimly lit room, the only visuals apparent to participants would be those on a patch of LCD screen underneath which their right hand would reside (see Figure 4). A monitor formed the roof of the box with the screen facing upwards and used to display the virtual hand. The monitor used In-Plane Switching (IPS) to allow for broad viewing angles of a 16.9x12.7cm area of screen with a resolution of  $\approx$ 102 pixels per inch. A Logitech C920 webcam was used to capture imagery of the hand at a resolution of 640x480 pixels and a frame rate of  $\approx$ 30Hz. The camera was attached immediately underneath the monitor on the inside of the box nearest to where the participant would be seated. The camera was directed at an angle facing the centre of the box, comparable to that of the participants’ gaze when looking at the virtual hand. The inside of the box was covered in black, grooved-rubber padding. This texturing provided a means by which participants could see a tangible background through the virtual hand when in a semi-transparent state. An LED lamp centred at the rear of the monitor illuminated the centre of the box.



**Figure 4. Participant “owns” her virtual hand under external guidance conditions.** All virtual hands were presented in the virtual box while EEG was recorded. For a full view of virtual hand stimuli see **Figure 5** on page 19. For the EEG electrode montage used, see **Figure 9** on page 28.

### 2.1.3 EEG Capture

EEG data was collected in an attempt to differentiate brain activity involved in the internal and external generation of perceptions of ownership and detachment of a virtual hand. An ANT Neuro system captured 32 channel EEG with Ag/AgCl electrodes positioned according to the 10-20 international system (Klem, Lüders, Jasper, & Elger, 1999) using a stretchable cap (Waveguard, ANT B.V., Enschede, The Netherlands, [www.ant-neuro.com](http://www.ant-neuro.com)). Electrodes captured were FP1, FPZ, FP2, F7, F8, F3, FZ, F4, FC5, FC1, FC2, FC6, T7, C3, CZ, C4, CP5, CP1, CP2, CP6, P7, P3, PZ, P4, P8, POZ, O1, OZ, O2 with M1 and M2 included as reference electrodes. An additional scalp electrode served as the ground electrode. The electrical impedance was maintained to below 7 k $\Omega$  through application of electroconductive gel and monitored using ASALAB 4.7 (ANT B.V., Enschede, The Netherlands, [www.ant-neuro.com](http://www.ant-neuro.com)).

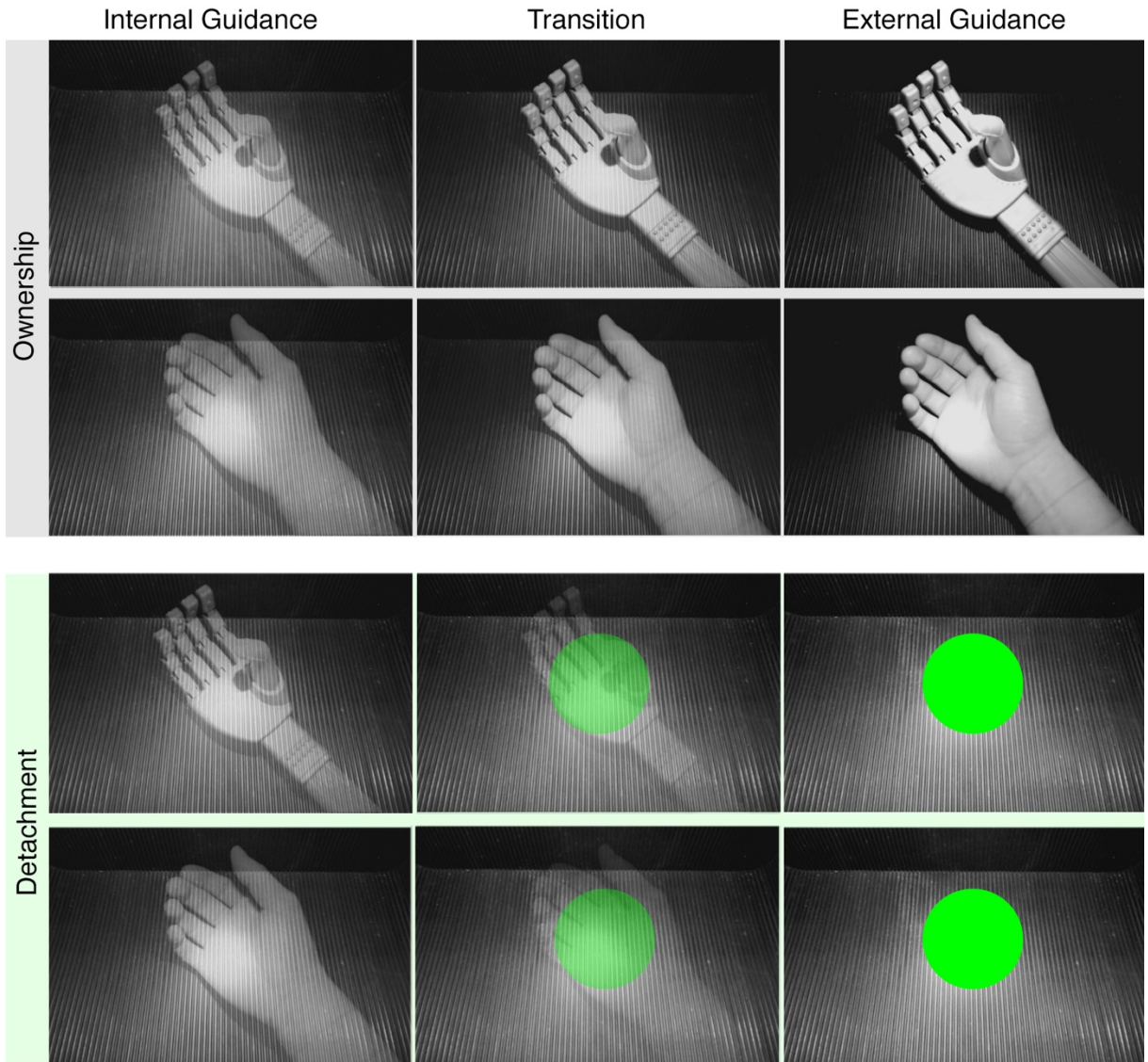


**Figure 5. Visual stimuli within the three trial phases across the focal conditions.** Top grey panel shows ownership stimuli and lower green panel shows detachment stimuli from the participant's perspective (screen captures). Each column shows the sequential phases within the trials with each lasting 7 seconds. **Left column:** internal guidance phase had neutral stimuli across ownership (**top two rows**) and detachment conditions (**lower two rows**). **Middle column:** The transition phase linearly transformed visual stimuli from that found under the neutral stimuli of internal guidance to distinct visual symbols used as external guides. **Right column:** The external guidance phase consisted of fully opaque representations of internal guides to aid evoking of ownership and detachment states. The virtual hand stimulus varied across type of either prosthetic (first and third rows) or human (second and fourth rows) virtual hands; and in half of the trials these hands were making small, clenching movements. In detachment trials, the green dot found in transition and external guidance phases of the trial (and imagined in the internal guidance phase) served as a distractor of attention away from the virtual hand while maintaining eye fixation within that of the area of virtual hand.

### 2.1.5 Verbal Instruction and Questions

#### Pre-experiment Instructions

With the experimental success being largely reliant on a participant's volitional internal engagement, it was imperative that the participant obtained a thorough understanding of the concepts of ownership, detachment and what they were expected to use as internal guidance. For the internal guidance phase participants were told it involves “*using your mind to alter your*

intended ownership perceptions, to my knowledge, is novel. Full description of the mathematical theory behind CSP analysis can be found in Appendix A2. Classifier Mathematics and Theory on page 91.

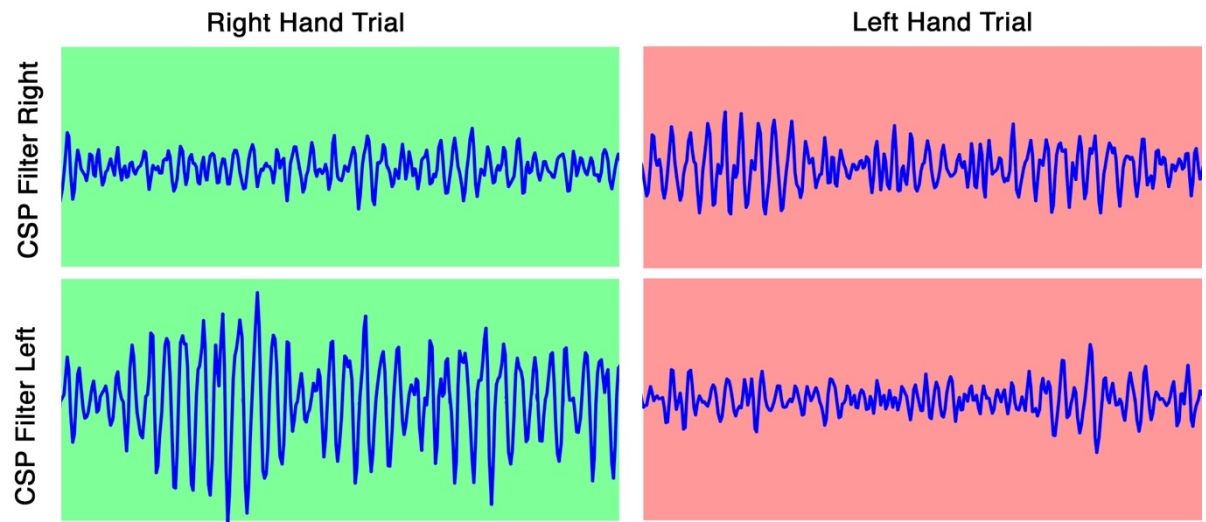


**Figure 7. Idealised CSP filtering example.** The effects of applying spatial filters derived using CSP analysis on band-pass filtered EEG can be seen above. The filters attempt to transform the EEG to maximally discriminate between the two conditions. **Left** column, green represents a transformed EEG segment taken from a trial of right hand imagery with **right** column, red being that of left hand imagery. Figure adapted from Blankertz et al. (2008).

## 2.2.2 Machine Learning Using Linear Discriminant Analysis

Linear Discriminant Analysis (LDA) is a simple and robust (Vidaurre et al., 2008) supervised machine-learning algorithm which was first introduced by (Fisher, 1936). LDA has proven to be a useful algorithm to classify mental states in EEG-based BCIs, although it can be limited by the presence of non-gaussian outliers (Blankertz et al., 2008; Muller, Anderson, & Birch, 2003; Vidaurre et al., 2008). LDA discriminates between two classes of data that are presumed to be normally distributed. The distribution curve is accepted to be identical for both classes with the prior probability of each class assumed to be equal. Effective pre-processing of the EEG data tends to transform the data to meet the normality assumptions. That is, appropriate epoching and band-pass filtering is needed which is followed by a logarithmic transformation – this transforms the distribution towards normality. Additionally, because the true distributions are unknown, the covariance matrices and means of the class distributions must also be estimated (Blankertz et al., 2009). We implemented a regularisation step called ‘shrinkage’ prior to LDA training to estimate the true distributions (Friedman, 1989). LDA training produces a linear midpoint vector and bias term for use in the final classification algorithm. The mathematical mechanisms by which this vector and bias term of the LDA algorithm is created is described in “LDA Weight Vector and Bias Creation” on page 93. Note that Support Vector

Machines is another commonly used classification algorithm available for classification, however it has not proven advantageous in CSP-based classification with issues of speed and overfitting (Li & Koike, 2011) as confirmed in a preliminary analysis in this study.

### 2.2.3 Classifier Implementation

Production and performance evaluation of classifiers to discern between internally-generated states of ownership and detachment provides a means to answer our primary question of interest – is an ownership and detachment biofeedback-training task feasible? Also, do humans produce a discernable biosignal when intending to own and detach from a virtual hand? If classification accuracy of the ownership–detachment calibration task exceeds that expected by chance, this suggests an online biofeedback paradigm is feasible. Therefore, all classification results were calculated in a manner that was compatible with online ('real-time') classification. To ensure a full assessment of robustness; no participants, trials or electrodes were excluded from analyses. Furthermore, an artefact rejection technique compatible with online methods were used.

### 2.2.4 Classification Pipeline

The accuracy of the classifications is dependent on six main stages in the classification pipeline. The first stage of the pipeline is the *production* of distinct physiological signals during the classified conditions during the calibration task – it is important these signals are consistently produced during all trials. Secondly, the differentiating signals are then *captured* – this capture is susceptible to inherent issues with EEG recording. Thirdly, the pertinent signals are *extracted* from the data – the latency of markers need be accurate and the correct epoch length allocated to allow for maximal extraction of the signal of interest with respect to noise. Fourthly, the artefact rejection, filtering and feature extraction algorithms attempt to *contrast* the relevant features with respect to the noise. Fifthly, an appropriate machine-learning algorithm is then applied to *separate* these characteristic features into a readily discernable feature space of which this algorithm may not be optimal. Sixthly, the online classification performance is *validated* using cross-validation testing of the classifier on 'unlabelled' EEG – this provides an estimate and is not a real-world measure of online performance success. Due to the imperfect nature of the EEG classification pipeline across all phases, in addition to the internal guidance dependence on participant engagement, the theoretical peak classification accuracy of 100% was not predicted. Therefore, the control stimuli and control electrode-cluster were implemented to indicate where along this pipeline any source of errors may have been produced. The first and second stages of the pipeline are described in the "Ownership-

## Methods – Is Biofeedback Training of Ownership Perceptions Possible?

Detachment Calibration Task” section. Description of steps three to six in the pipeline and an explanation of the controls follow below. For a full overview of the classification pipeline see Figure 8 below.

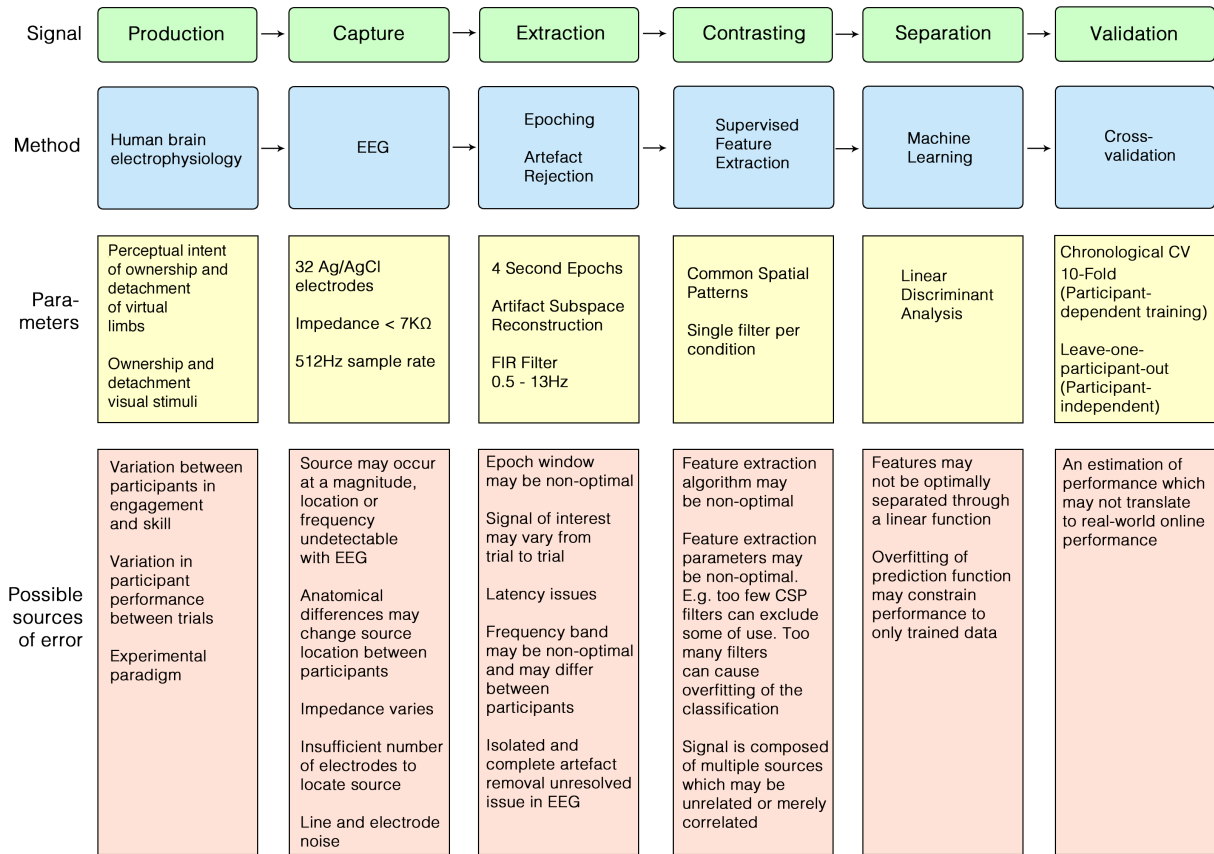


**Figure 8. Overview of classification pipeline used to classify ownership-detachment.** Each column represents a different stage in the pipeline in chronological order (left to right). The parameter row (third row from top) shows the specific parameters used in this calibration paradigm whereas the other rows are mostly relevant to EEG classification in general. The last row shows possible sources of classification error, of which error at any point of the pipeline will have a ‘knock-on’ effect on the following stages.

### 2.2.5 Classification Regimes

#### Guidance Stimuli

The classification of *intent* of ownership (internal guidance) was subject to uncertainty in performance. This is because the EEG source of ownership intent, while inferred, has not specifically been demonstrated. Moreover, the production of this signal was at least partially dependent on individual engagement and skill which varies from person to person. Therefore, external guidance stimuli served as a critical control to ensure EEG extraction and classification methods were valid. This purpose was in addition to its role as a symbolic reinforcer and simulation of feedback (see Visual Stimuli, page 17). The external guidance epochs were specified as the four seconds once the external guides were fully opaque and given a buffer of 1.8 seconds before the participants were asked to close their eyes. The internal guidance epochs

the classifier (extract features and create the unique prediction function) while the remaining part was used to test the performance of this classifier on the test set. The splitting of data occurred in chronological fashion such that each trial was a member of the test set on only one occasion and trials were presented in sequential order. Chronological training is commonly used in BCI classification due to the characteristic nonstationarity of the EEG signal over time (Dornhege, 2007) allowing a more accurate estimation of biofeedback performance from offline to online sessions. Under participant-independent training, a leave-one-participant-out regime was used where, for each fold one participant was excluded from the training set and formed the test set. The mean success rate across each participant's classification gave the performance estimate for a particular regime. Similarly, the successful classification of ownership trials and detachment trials was calculated independently to reveal any biases of the classifiers. Note that individual classification values are comparable between participant-dependent and participant-independent classification as the test set is confined to that of an individual.

### Random Success Distribution

The performance of an ownership–detachment classifier must be evaluated while considering that expected of a random binary classifier. If a classifier's performance is equivalent to that of a random classifier, we expect the probability of successful classification of a single trial to be that of a Bernoulli trial. That is, in a random binary classifier let  $y$  represent a single-trial with a possible binary outcome of 1 (success) or 0 (failure). The outcome of each trial may be represented as  $P(y_i = 1) = \pi$  and  $P(y_i = 0) = 1 - \pi$  with probability of success  $\pi$  (Agresti & Kateri, 2011). With the trial order randomized it would be expected the probability of success of a random binary classifier on a single trial to be that of a fair-coin toss with  $\pi = 0.5$ . Repeating this Bernoulli trial  $n$  times – as in the case of classifier performance evaluation – we would then expect a binomial performance distribution of success in a classification regime producing chance performance.

### Expected Population Distribution of Classification Regime Performance

A classifier's performance across a population of Bernoulli trials would mimic that of a binomial distribution. In such a distribution of  $y_1, y_2, \dots, y_n$  unlabelled, independent trials with population  $n$ , the distribution of a random classifier's number of successes would follow the binomial distribution with the probability mass function for the possible number of successes  $y$  for the distribution  $Y$  is shown in the below equation with the binomial coefficient represented

by  $\binom{n}{y} = \frac{n!}{[y!(n-y)!]}$  and  $E(Y_i) = \pi$  and  $var(Y_i) = \pi(1 - \pi)$ . Allow  $Y = \sum_{i=1}^n Y_i$  to represent the binomial distribution with mean  $\mu = E(Y)$  and  $var(Y) = \pi(1 - \pi)$  (Agresti & Kateri, 2011). The probability max function is then represented in the equation below.

$$p(y) = \binom{n}{y} \pi^y (1 - \pi)^{n-y}, \quad y = 0, 1, 2, \dots, n$$

The performance distribution of a random ownership–detachment classification regime would follow the above binomial distribution with  $\pi = 0.5$ . A simulation of 1000 such random distributions was conducted using the R function *rbinom* (see Figure 10 below). Parameters were selected to match the present paradigm’s methods. Parameters encode for a population of 35 accuracy values distributed according to 26 ‘fair-coin tosses’ (Bernoulli trials). These simulations demonstrate random binomial distributions within the current paradigm parameters.

## Methods – Is Biofeedback Training of Ownership Perceptions Possible?

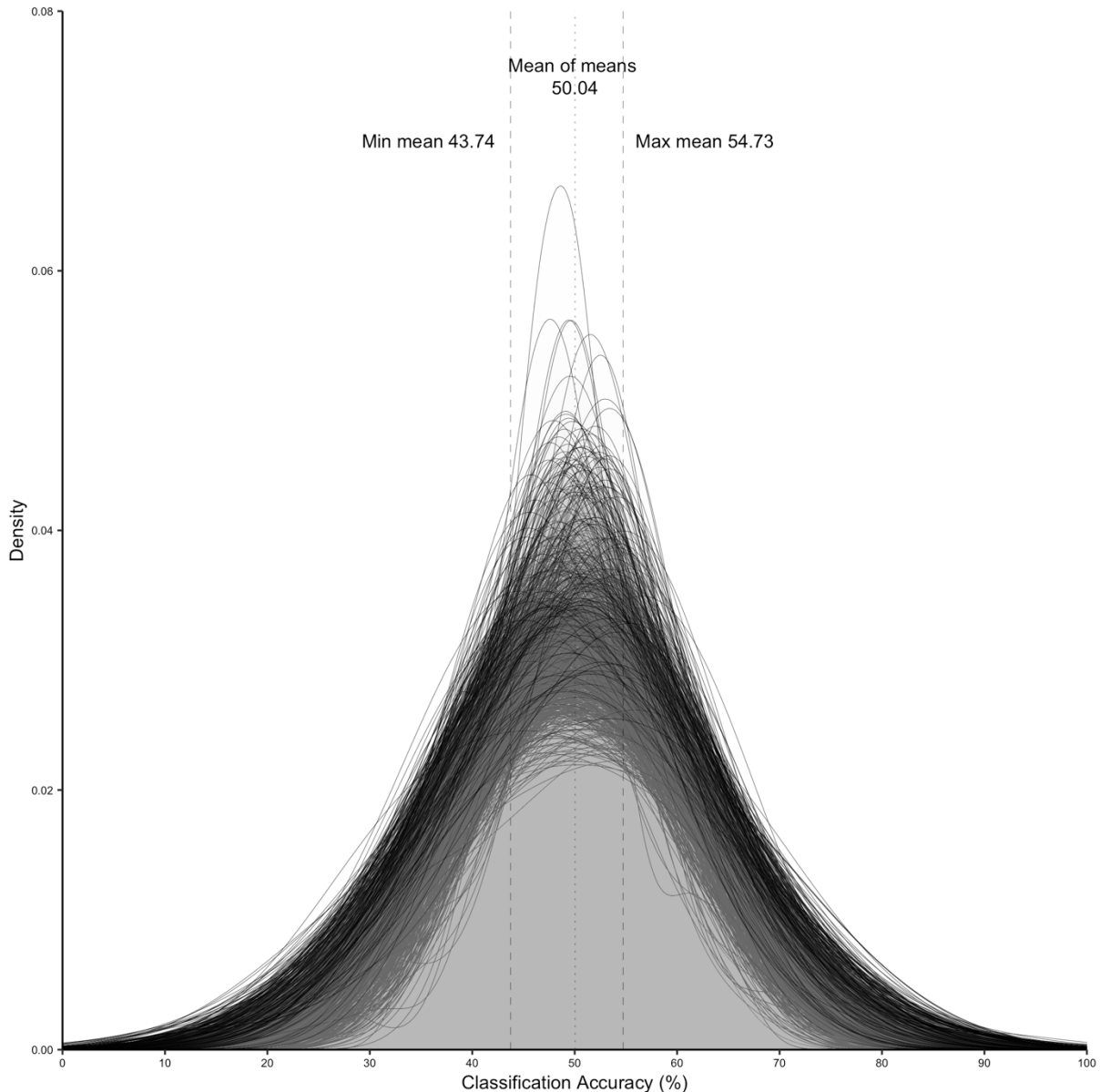


**Figure 10. Simulation of 1000 Random Binomial Distributions.** Distributions were simulated with populations matching the current experimental methods. The minimum and maximum means found across the distributions were 43.74% and 54.73% respectively.

### Statistical Analyses

One-sample t-tests assessed mean classifier performance against that of 50% to test whether a classification regime outperformed binary chance classification. Multiple comparisons were corrected for using a Bonferroni correction. Distribution plots were used to allow visual comparison of how factors of guidance and training effected the classifier accuracy distributions. The ggplot2 distribution plotting function geom\_density was used for kernel density distribution plotting. For improved viewability, the bandwidth smoothing parameter of these plots were set with a multiplier of 2. Correlation fitting of the participant-independent-participant-dependent and internal-external classification was performed using Pearson's

## Results – Is Biofeedback Training of Ownership Perceptions Possible?

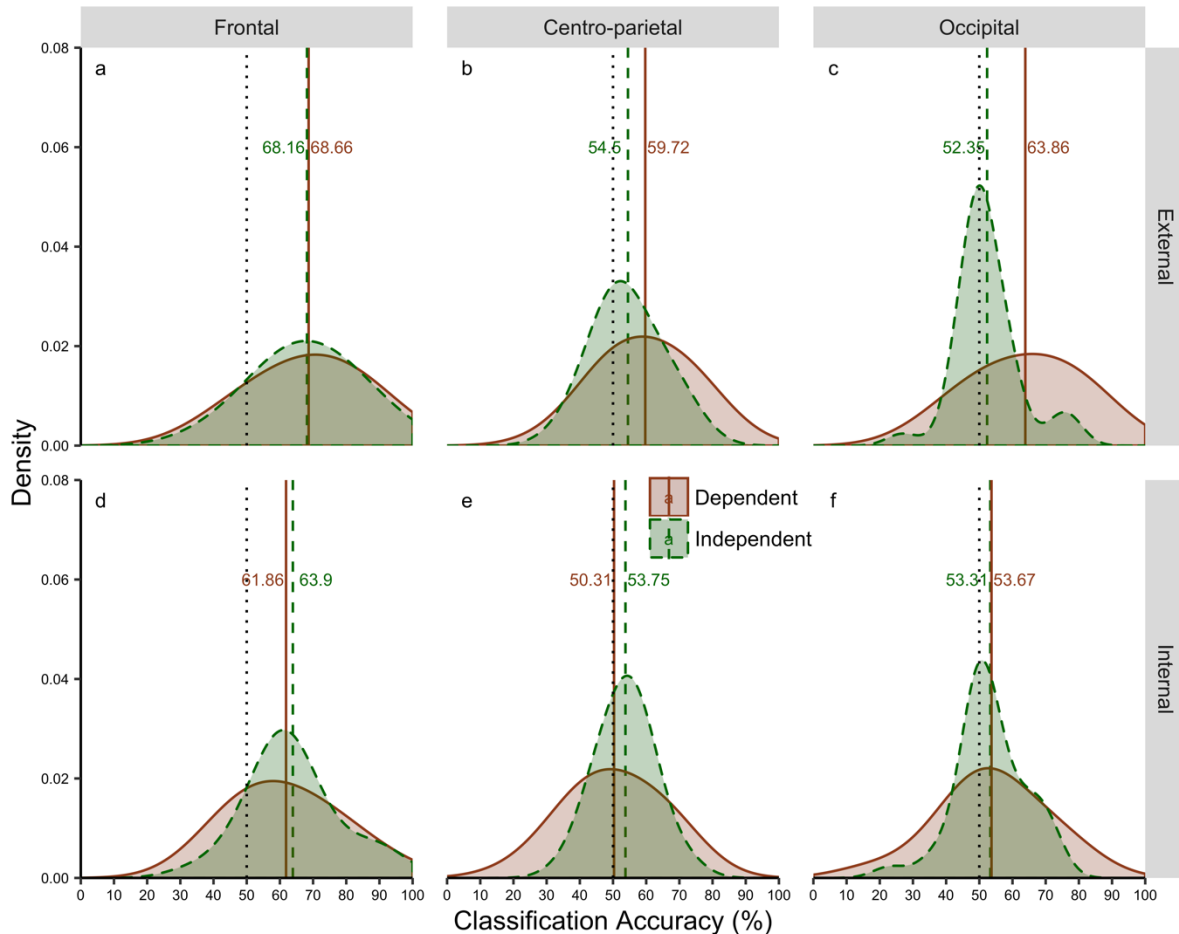


**Figure 11. Kernel density distribution plot for participant-independent and participant-dependent training methods.** All panels represent the distribution of discriminatory performance across participants for participant-independent (brown, solid line) and participant-dependent (green, dashed line) training. Chance performance is represented as the dotted black line (50%). N=35 for each distribution. Upper row represents those classifiers trained under external guidance; lower row represents those trained under internal guidance. Left to right columns shows classifiers confined to frontal, centro-parietal and occipital electrodes, respectively. The y-axis shows kernel density of participants falling within the corresponding accuracy on the x-axis. Mean performance of the distribution is shown by the vertical dashed dotted lines in the colour corresponding to the participant-independent or participant-dependent training regimes. The narrower range of participant-independent-trained classification is evident, as too is the accuracy improvement for participant-dependent over participant-independent distributions for the centro-parietal cluster under external conditions. The frontal cluster shows a unique overlap of participant-independent participant-dependent distributions for external guidance.

### 3.3.2 Internal and External Distributions

Distribution plots of external and internal conditions illustrate the effect of guidance stimulus on performance across participants. While Figure 11 (above) is most indicative of reliability of participant-independent and participant-dependent training methods across participants, Figure 12 (next page) enables comparison of the effect of guidance stimuli under the various regimes. Most noticeable is the repeated and uniform positive shift in performance from internal to external guidance distributions under participant-dependent training as was hypothesised. External guidance consistently produced the best performing discrimination scores across these three classification regimes (Figure 12, d-f). It can be seen that the performance increase from internal to external guidance for the centro-parietal ‘bottom-up’ cluster was relatively greater

## Results – Is Biofeedback Training of Ownership Perceptions Possible?

than that of the frontal ‘top-down’ cluster as was expected; this was the case only for the significant performing participant-dependent centro-parietal classification.

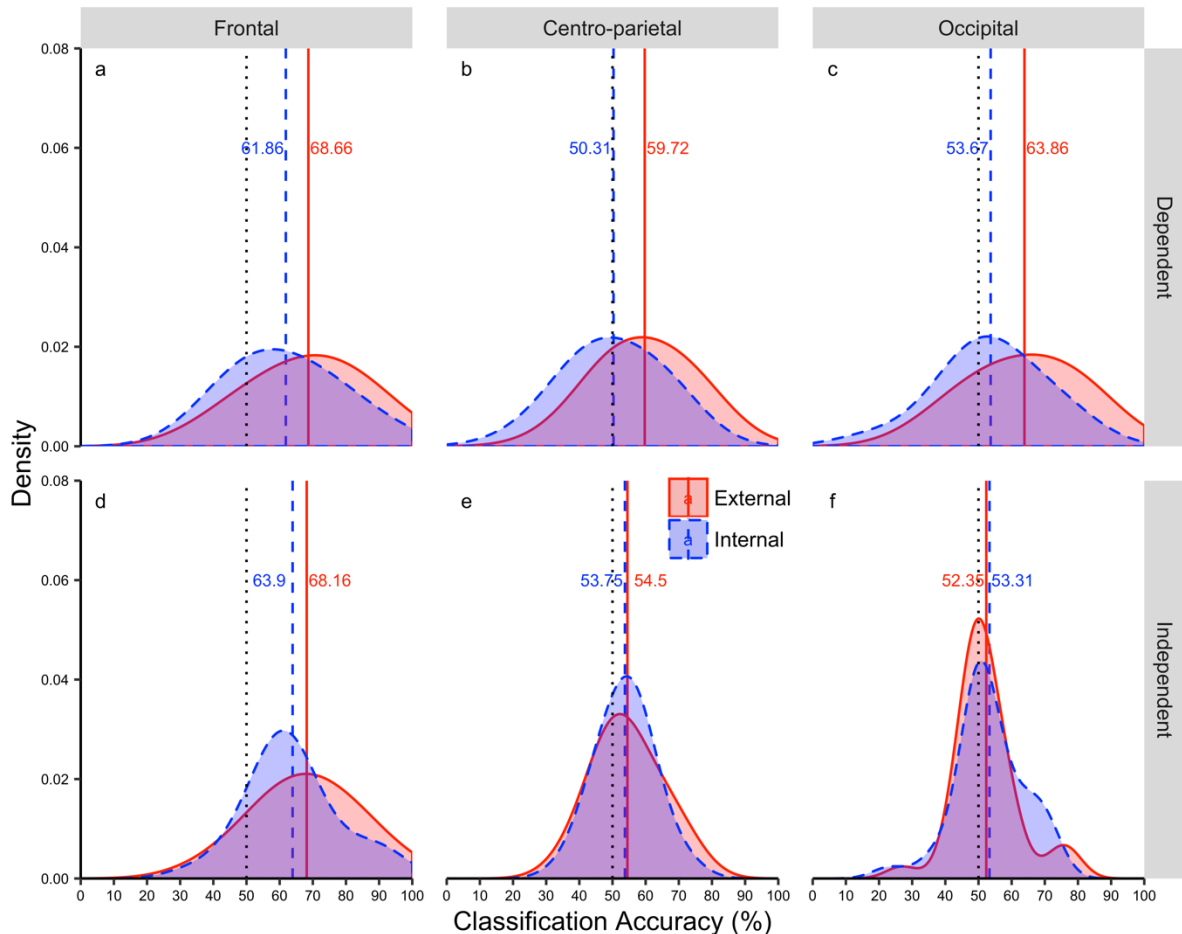


**Figure 12. Kernel density distribution plot for Internal and External Guidance.** Each distribution shows discriminatory performance across participants for external (red) and internal (blue) guidance. **Top** row shows classifiers trained on whole participant-independent; **lower** row shows those trained using participant-dependent training. Columns show classifiers confined to frontal (**left**), centro-parietal (**middle**) and occipital (**right**) electrode clusters. The y-axis shows kernel density of participants falling within the corresponding accuracy on the x-axis. Mean accuracy is shown by the vertical lines. Random binary classifier performance is shown as the dotted black line (50%). N=35 for each distribution. A clear positive shift in external over internal distributions is consistently found for participant-dependent training (**panel d-f**) as was hypothesised.

### 3.4 Correlations

Correlation fittings of training method (participant-independent–participant-dependent) and guidance stimuli (internal–external) were performed to further guide the methods of online implementation. Correlations were analysed using Pearson’s product-moment correlation and Bonferroni corrected for multiple comparisons.

### 3.4.1 Participant-independent–Participant-dependent Performance

Correlation fitting of the participant-independent–participant-dependent classification accuracy assessed the reliability of classifier training method to guide implementation of the classifier in an online paradigm (see Figure 13). The frontal cluster produced the most reliable results with the largest correlations under both levels of guidance stimuli [external  $r(33) = .82$ , internal  $r(33) = .69$ ,  $p < .0001$ ; Figure 13a and d], suggesting a strong robustness of classification performance across participant-independent and participant-dependent trainings. Those correlations for the centro-parietal region were shallower, with a significant correlation for external [ $r(33) = .70$ ,  $p < .0001$ , Figure 13b] but not internal [ $r(33) = .12$ ,  $p > .5$ , Figure 13e] guidance conditions. Similarly, the occipital region found significant correlation between participant-independent–participant-dependent training under external [ $r(33) = .42$ ,  $p < .05$ , Figure 13c] but not internal [ $r(33) = .22$ ,  $p > .5$ , Figure 13f] guidance phases.

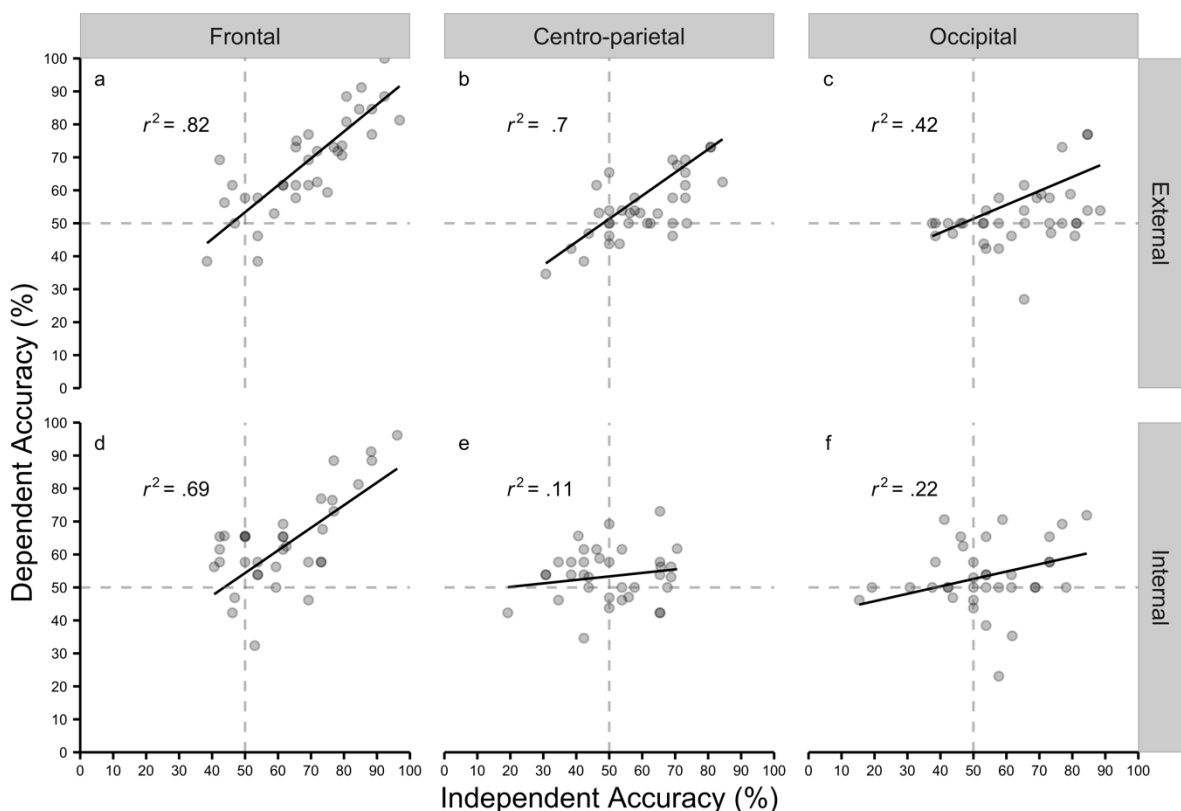


**Figure 13. Participant-independent–participant-dependent training scatterplot of participant performance.** Panels are arranged with top row (a-c) for external guidance, bottom row (d-f) for internal guidance; **left:** frontal, **middle:** centro-parietal and **right:** occipital. These plots show the correlation ( $r^2$ ) in classification performance between participant-independent (x-axis) and participant-dependent (y-axis) training across each participant. Dashed grey lines represent chance performance (50%). Significant positive correlations were found for the frontal cluster for both internal (panel d) and external (panel a) guidance ( $p < .0001$ ). Additionally, under the ‘bottom-up’ external phase of the trial, significant correlations were found in the centro-parietal ( $p < .0001$ , panel b) and occipital ( $p < 0.001$ , panel c) clusters; but not under the ‘top-down’ internal phase of the trial (panel e and f).

## Results – Is Biofeedback Training of Ownership Perceptions Possible?

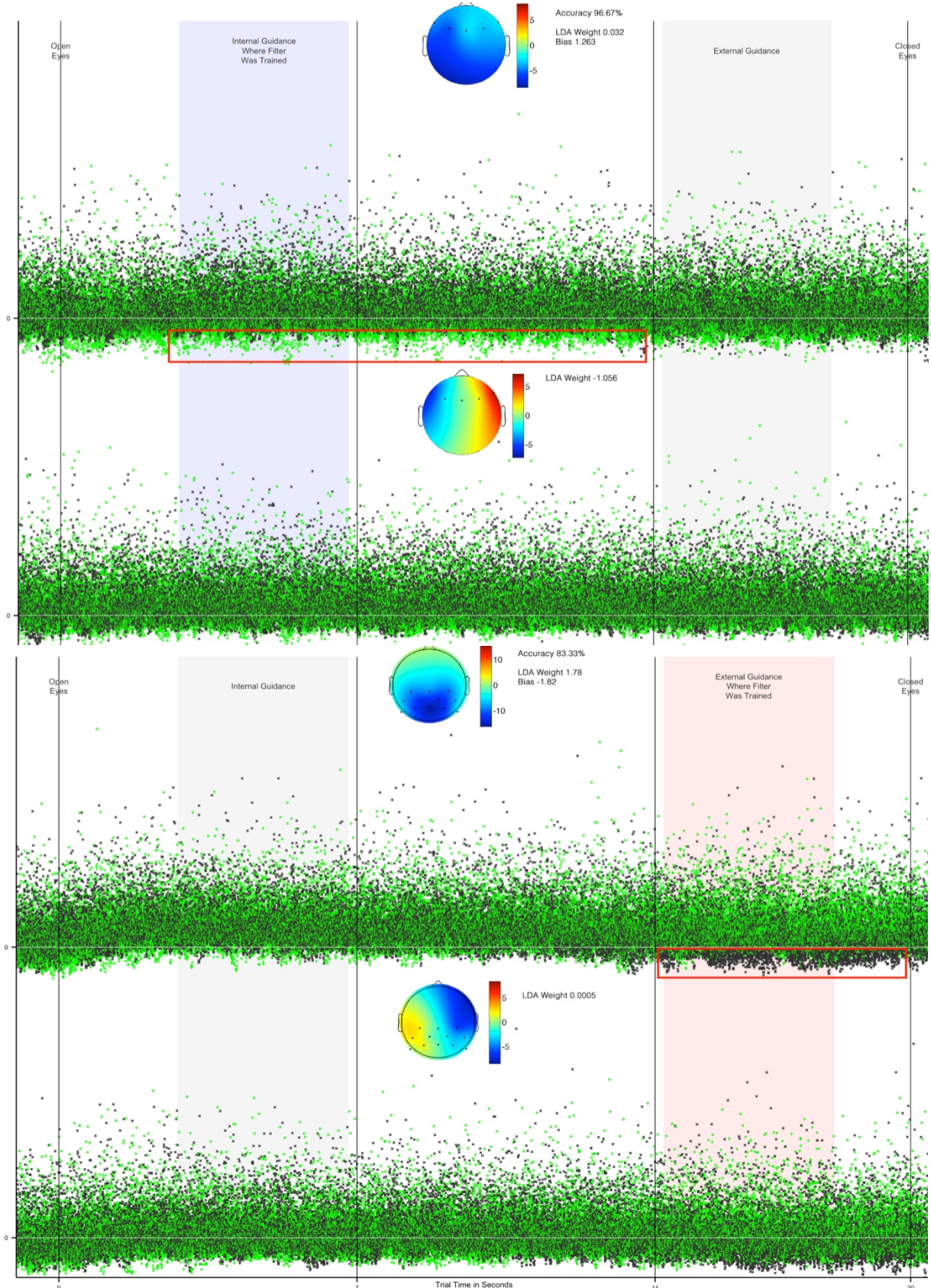


**Figure 18. Participant-dependent feature space.** **Top:** C29 internal frontal, **upper** CSP causes detachment features to project negatively (below white line at  $y=0$ , red rectangle) however, machine-learning algorithm finds this feature space redundant as shown by the LDA weight of 0.032. **Bottom:** C12 external centro-parietal, **upper** external CSP produces a distinct ownership feature space (red rectangle) under external guidance (projected negatively). This filter uses an occipital source as to be expected under distinct visuals. **Lower** CSP is less useful for classifier, both visually and shown by LDA weight of 0.0005.

## Results – Is Biofeedback Training of Ownership Perceptions Possible?

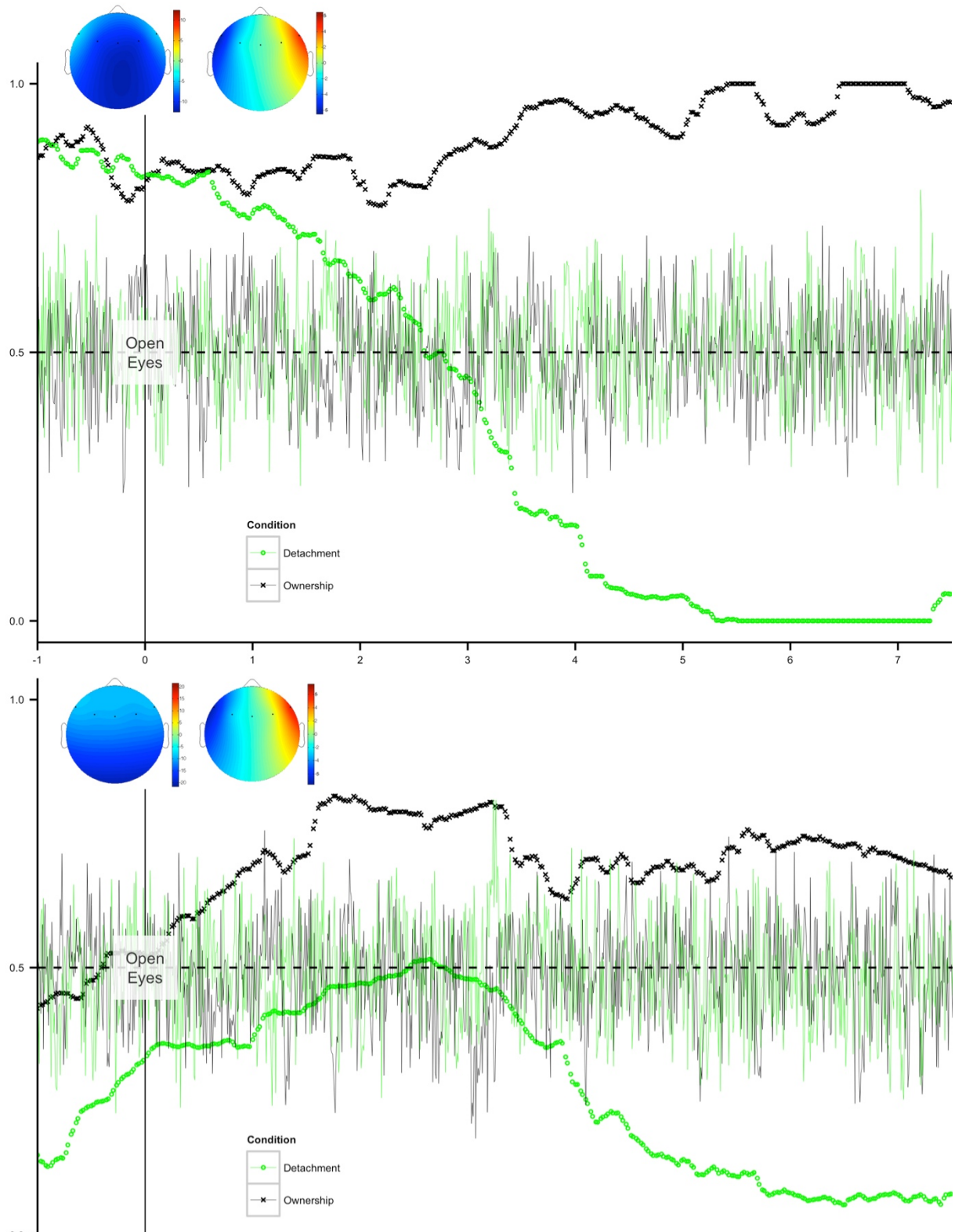


**Figure 19. Online classification simulation for top-performers using participant-independent, frontal regime.** CSP plots for the respective classifiers are top left. The x-axis represents trial time in seconds and y-axis shows classifier prediction. Each green circle (detachment) and black cross (ownership) is a mean probability prediction by the classifier on previously unseen EEG over 13 trials. The line plot shows EEG the classifier received as input (averaged, normalised for viewability). **Note:** Dashed line ( $y = .5$ ) is predictor threshold; all black crosses of  $y > .5$  and green dots of  $y < .5$  are correct mean predictions. These participant-independent classifiers were trained with the respective participant's data excluded. Predictions have been offset by 2 seconds of prediction delay. **Upper:** C29's classification shows a clear and accurate predictor divergence between ownership-detachment data soon after the trials begin. **Lower:** C34's predictor begins with a small, although discriminable difference between ownership-detachment data; similarly to C29 this separation is accurately amplified as the trials progress.

## Discussion – Is Biofeedback Training of Ownership Perceptions Possible?

The present paradigm's data capture and classification methods can successfully elicit and distinguish between ownership–detachment intentions. This in turn suggests people have the capability to alter their ownership intent and this intent is expressed in a distinguishable biosignal. CSP analysis pointed toward saccadic activity as being a useful discriminating source, leading to ICA that suggests that in a visual ownership perceptual paradigm, ownership intent increases saccadic activity when compared with intent to detach. The conducting of a similar ownership paradigm to the present with the inclusion of eye-tracking apparatus will give precise insight into this phenomenon; as to the best of my knowledge, such an investigation has not been conducted. Regardless, this difference in saccadic activity, while not the origins of ownership perception itself, is nonetheless likely reflective of ownership intent and part of the functional mechanisms which allow for ownership perception; this is due to the fact that the desired perception has an explicit relationship to the visual stimulus – the ownership of a visual stimulus, a virtual hand. Hence, saccadic activity is possibly the most currently applicable physiological metric of *intention* of ownership of a visual stimulus such as a virtual hand. This finding, taken in conjunction with the self-reported findings of a positively correlated change in internal engagement with ownership perception implies saccadic training may be a method to enhance levels of perceived ownership of visual objects such as virtual hands.

## 5 REFERENCES

- Acqualagna, L., Bosse, S., Porbadnigk, A. K., Curio, G., Müller, K.-R., Wiegand, T., & Blankertz, B. (2015). EEG-based classification of video quality perception using steady state visual evoked potentials (SSVEPs). *Journal of neural engineering*, 12(2), 026012.
- Agresti, A., & Kateri, M. (2011). *Categorical data analysis*: Springer.
- Arns, M., de Ridder, S., Strehl, U., Breteler, M., & Coenen, A. (2009). Efficacy of neurofeedback treatment in ADHD: the effects on inattention, impulsivity and hyperactivity: a meta-analysis. *Clinical EEG and neuroscience*, 40(3), 180-189.
- Aron, A. R., Fletcher, P. C., Bullmore, E. T., Sahakian, B. J., & Robbins, T. W. (2003). Stop-signal inhibition disrupted by damage to right inferior frontal gyrus in humans. *Nature neuroscience*, 6(2), 115-116.
- Asada, H., Fukuda, Y., Tsunoda, S., Yamaguchi, M., & Tonoike, M. (1999). Frontal midline theta rhythms reflect alternative activation of prefrontal cortex and anterior cingulate cortex in humans. *Neuroscience letters*, 274(1), 29-32.
- Bengtsson, H., Jacobson, A., Riedy, J., Bengtsson, M. H., LazyLoad, T., & ByteCompile, T. (2015). Package 'R. matlab'.
- Blankertz, B., Sannelli, C., Halder, S., Hammer, E. M., Kübler, A., Müller, K.-R., . . . Dickhaus, T. (2010). Neurophysiological predictor of SMR-based BCI performance. *Neuroimage*, 51(4), 1303-1309.
- Blankertz, B., Tangermann, M., Vidaurre, C., Dickhaus, T., Sannelli, C., Popescu, F., . . . Müller, K.-R. (2009). Detecting mental states by machine learning techniques: The Berlin brain-computer interface *Brain-Computer Interfaces* (pp. 113-135): Springer.
- Blankertz, B., Tomioka, R., Lemm, S., Kawanabe, M., & Muller, K.-R. (2008). Optimizing spatial filters for robust EEG single-trial analysis. *Signal Processing Magazine, IEEE*, 25(1), 41-56.
- Blom, R. M., Hennekam, R. C., & Denys, D. (2012). Body integrity identity disorder. *PloS one*, 7(4), e34702.
- Bonmassar, G., Anami, K., Ives, J., & Belliveau, J. W. (1999). Visual evoked potential (VEP) measured by simultaneous 64-channel EEG and 3T fMRI. *Neuroreport*, 10(9), 1893-1897.
- Bouchard, S., Bernier, F., Boivin, É., Morin, B., & Robillard, G. (2012). Using biofeedback while immersed in a stressful videogame increases the effectiveness of stress management skills in soldiers. *PloS one*, 7(4), e36169.
- Buschman, T. J., & Miller, E. K. (2007). Top-down versus bottom-up control of attention in the prefrontal and posterior parietal cortices. *Science*, 315(5820), 1860-1862.
- Cabeza, R., Ciaramelli, E., & Moscovitch, M. (2012). Cognitive contributions of the ventral parietal cortex: an integrative theoretical account. *Trends in cognitive sciences*, 16(6), 338-352.
- Cahn, B. R., Delorme, A., & Polich, J. (2010). Occipital gamma activation during Vipassana meditation. *Cognitive processing*, 11(1), 39-56.
- Cavanagh, J. F., & Frank, M. J. (2014). Frontal theta as a mechanism for cognitive control. *Trends in cognitive sciences*, 18(8), 414-421.
- Cerf, M., Thiruvengadam, N., Mormann, F., Kraskov, A., Quiroga, R. Q., Koch, C., & Fried, I. (2010). On-line, voluntary control of human temporal lobe neurons. *Nature*, 467(7319), 1104-1108.
- Chan, B. L., Witt, R., Charrow, A. P., Magee, A., Howard, R., Pasquina, P. F., . . . Tsao, J. W. (2007). Mirror therapy for phantom limb pain. *New England Journal of Medicine*, 357(21), 2206-2207.
- Chen, Y., Huang, H., Xu, W., Wallis, R. I., Sundaram, H., Rikakis, T., . . . He, J. (2006). *The design of a real-time, multimodal biofeedback system for stroke patient rehabilitation*. Paper presented at the Proceedings of the 14th annual ACM international conference on Multimedia.

## Appendix A2. Classifier Mathematics and Theory

Each generated classifier can be represented as a prediction function  $f$  as in Equation 1, with  $w$  and  $\beta$  being unique constants as determined by feature extraction and machine learning while  $X$  represents a window of EEG. Here, the segment  $X$  of EEG samples is in matrix form of  $C \times T$  with  $C$  representing the number of channels and  $T$  the number of timepoints. The spatial filters extracted during CSP feature extraction are represented in the weight matrix  $\{w_j\}_{j=1}^J$  with the length of each vector  $w_j$  being that of the number of channels  $C$  with the linear weights derived through LDA are represented by  $\{\beta_j\}_{j=0}^J$ . The bias term  $\beta_0$  represents a single value and also is determined through LDA (Blankertz et al., 2008). The final output of the predicted condition label is in the range of  $> 1$  for ownership and  $< -1$  for detachment.

$$f(X; \{w_j\}_{j=1}^J, \{\beta_j\}_{j=0}^J) = \sum_{j=1}^J \beta_j \log(\text{var}(w_j^\top X^\top X w_j)) + \beta_0 \quad (1)$$

The CSP filters used to transform the EEG into discriminable features are now mathematically described. Let CSP channel filters be represented in the matrix form  $W^{C \times C}$  with  $C$  representing the number of channels. Each column vector represents a spatial filter, which projects the original signal into surrogate channel space. Hence one can only produce as many CSP filters as there are channels. The inverse of the CSP filter matrix ( $W$ ) yields the source pattern ( $W^{-1}$ ) of the CSP filter and allows for physiological interpretation of the invariant sources of interest. Possible mechanisms by which the CSP filters are trained from the EEG are through solving an optimisation problem, a geometric approach using Principal Component Analysis or eigen-vector analysis (C. A. Kothe, 2013). We will now describe the CSP creation variant of eigen-vectors because eigen-vector analysis in MATLAB is the simplest to implement with low computational cost (C. A. Kothe, 2013) and was used in the present study in the manner detailed by (Blankertz et al., 2008) and described below.

The creation of discriminatory CSP filters begins with those steps typical of that of a common band-power analysis. Even though CSP analysis is ultimately applied as a spatial filter, because these filters are derived from signal variance and because variance of a band-pass signal is equal to band-power, this makes CSP dependent on changes in oscillatory power within the frequency range of the band-pass filter. Therefore, as a first step, an FIR band-pass filter is applied to the data. Secondly, the EEG dataset is partitioned in two with each set composed of time-series EEG from trials of a labelled condition. In our perceptual state discrimination

analysis, allow  $X^O$  to represent EEG obtained from ownership trials and  $X^D$  to represent detachment EEG both having C channels, T time points and N trials.

$$X^{Cond} \in \mathbb{R}^{C \times T \times N} \quad (Cond \in \{O, D\})$$

Next, the covariance matrices for each condition of the above EEG are estimated. The standard manner to obtain covariance matrices is shown in Equation 2. The present method employed a robust variant of this equation called analytical shrinkage (Schäfer & Strimmer, 2005) through the BCILAB function cov\_shrink.m. In Equation 2,  $N_{Cond}$  represents the number of trials pertaining to either of the binary conditions ( $Cond \in \{O, D\}$ ). These covariance matrices transform the EEG into a format allowing for the definitive step of the CSP analysis.

$$\Sigma^{(Cond)} = \frac{1}{|N_{Cond}|} \sum_{i \in N_{Cond}} X_i X_i^\top \quad (Cond \in \{O, D\}) \quad (2)$$

The defining step of a CSP filter ( $W$ ) creation involves the concurrent diagonalisation of the covariance matrices that creates a filter enabling dispersion of channel data maximally for one class and minimally for the other class. In equation 3,  $\Lambda$  represents the diagonals of these matrices with  $W$  scaled so that  $\Lambda^O + \Lambda^D = I$  (as introduced by (Fukunaga, 1990)).

$$W^\top \Sigma^O W = \Lambda^O \quad W^\top \Sigma^D W = \Lambda^D \quad (3)$$

The above step can be simplified by computing the generalized eigenvalue problem of equation 4 which is done in BCILAB using MATLAB's eig() function.

$$\Sigma^O w = \frac{\lambda^O}{\lambda^D} \Sigma^D w \quad (4)$$

Here all  $\frac{\lambda^O}{\lambda^D}$  represents the variance in the respective surrogate channel with  $\lambda^{Cond} \geq 0$  and  $\lambda^O + \lambda^D = 1$  to form a linear contrast of the signal for the two classes. Those filters with a high  $\lambda^O$  and correspondingly low  $\lambda^D$  for a particular channel strongly discriminate the EEG by producing a surrogate signal with a large variance if in an ownership trial and low variance if in a detachment trial. By applying these filters trial independence is magnified and an orthogonal decorrelation of the two signals is achieved. These eigenvectors represent the spatial filters, with a subset of eigenvectors used from each end of the eigenvalue spectrum to reduce the dimensionality of the data.

Spatial patterns, the inverse of the CSP filters allow for physiological interpretation (Haufe et al., 2014) of features used in classification results. The spatial patterns of CSP are a fixed representation of the sources that are used to discriminate between the EEG representing the two conditions. These spatial patterns are readily created through finding the inverse of the CSP spatial filters as shown in equation 5 (Blankertz et al., 2008). Let  $A$  equal the set of spatial patterns and  $W$  the set of spatial filters as derived in the previous section and  $C$  the number of channels. Finding the inverse of the matrix of spatial filters and transforming this matrix derives the set of corresponding spatial patterns.

$$A = (W^{-1})^\top \in \mathbb{R}^{C \times C} \quad (5)$$

To supply the machine-learning algorithm of LDA and the final prediction function with the discriminatory features, the created CSP filters are applied to the EEG as per equation 6. A particular trial epoch  $t$  is reduced in dimensionality by applying the spatial filters to the respective number of EEG samples  $\tau$  by the number of spatial filters  $J$ . Calculation of the variance of these features and subsequent application of the logarithm reduces the feature matrix to a single value per spatial filter per trial.

$$F_t^J = \log(\text{var}(W^\top X)) \quad (6)$$

### LDA Weight Vector and Bias Creation

Linear Discriminant Analysis (LDA) involves training of separate class features produced by CSP filtering of the EEG. LDA training function produces the LDA weight vector  $W$  through Equation 7 with features extracted from ownership trials,  $F^O$  and features extracted from detachment trials,  $F^D$ .  $W$  is transformed into  $\beta$  and subsequently the bias term  $\beta_0$  used in the final prediction function (described above). Shrinkage estimation of the covariance matrices produces  $\text{var}(F^O)$  and  $\text{var}(F^D)$ .

$$\mu^{OD} = \frac{\mu^O + \mu^D}{2}$$

$$\text{var}(F^{OD}) = \frac{\text{var}(F^O) + \text{var}(F^D)}{2}$$

$$W = \frac{\mu^O - \mu^D}{\text{var}(F^{OD})} \quad (7)$$

Appendices – Is Biofeedback Training of Ownership Perceptions Possible?

$$\beta = \frac{W}{(\mu^D - \mu^{OD}) \times W'}$$

$$\beta_0 = \mu^{OD} \times \beta^\top$$